

# Environmental effects of H<sub>2</sub>O on fracture initiation in silicon: A hybrid electronic-density-functional/molecular-dynamics study

Shuji Ogata<sup>a)</sup>

*Department of Applied Sciences, Yamaguchi University, Ube 755-8611, Japan*

Fuyuki Shimojo

*Department of Physics, Kumamoto University, Kumamoto 860, Japan*

Rajiv K. Kalia, Aichiro Nakano, and Priya Vashishta<sup>b)</sup>

*Collaboratory for Advanced Computing and Simulations, Department of Material Science & Engineering, Department of Physics & Astronomy, Department of Computer Science and Department of Biomedical Engineering, University of Southern California, Los Angeles, California 90089-0242*

(Received 20 June 2003; accepted 3 February 2004)

A hybrid quantum-mechanical/molecular-dynamics simulation is performed to study the effects of environmental molecules on fracture initiation in silicon. A (110) crack under tension (mode-I opening) is simulated with multiple H<sub>2</sub>O molecules around the crack front. Electronic structure near the crack front is calculated with density functional theory. To accurately model the long-range stress field, the quantum-mechanical description is embedded in a large classical molecular-dynamics simulation. The hybrid simulation results show that the reaction of H<sub>2</sub>O molecules at a silicon crack tip is sensitive to the stress intensity factor  $K$ . For  $K=0.4\text{ MPa}\cdot\sqrt{\text{m}}$ , an H<sub>2</sub>O molecule either decomposes and adheres to dangling-bond sites on the crack surface or oxidizes Si, resulting in the formation of a Si–O–Si structure. For a higher  $K$  value of  $0.5\text{ MPa}\cdot\sqrt{\text{m}}$ , an H<sub>2</sub>O molecule either oxidizes or breaks a Si–Si bond. © 2004 American Institute of Physics. [DOI: 10.1063/1.1689004]

## I. INTRODUCTION

To address environmental concerns and to increase the efficiency of thermal and chemical processes, there is an increasing need<sup>1</sup> to use various kinds of ceramic and semiconductor components in chemically and physically harsh environments. Feature sizes of useful components in microelectromechanical systems (MEMS)<sup>2,3</sup> and electronic devices<sup>3</sup> are becoming smaller, reaching nanometer ranges.<sup>3–5</sup> Their large surface-to-volume ratios make the components more susceptible to environmental effects. For example, a MEMS-based mechanical testing<sup>6</sup> has shown the existence of fatigue (i.e., crack growth under repeated subcritical loading) at a submicron-sized crack in Si, although there is no fatigue in bulk Si. This unexpected result may be related to the oxidation of the Si crack tip. These small components are utilized for applications in which their lifetime prediction is crucial.<sup>2,3</sup> Theoretical lifetime prediction based on usual “universal” scaling laws<sup>1</sup> may be inapplicable to such small-feature-sized systems. One of the outstanding problems in theoretical lifetime prediction is to understand effects of environmental molecules<sup>1,7</sup> on fracture initiation. It is well known<sup>7–11</sup> that environmental H<sub>2</sub>O molecules significantly enhance crack growth in strained silica glasses through their chemical reactions<sup>12,13</sup> with silica: Si–O–Si

+ H<sub>2</sub>O → Si–OH + HO–Si. Other molecules, such as ammonia and hydrazine, also enhance crack growth in silicate glasses<sup>7</sup> as well as in alumina.<sup>7</sup>

Since Si is a crucial element of many important electronic devices and its atomic structure is well known, crystalline Si is a suitable system for studying chemical reactions with environmental molecules.<sup>14</sup> A report<sup>15</sup> exists on environmentally enhanced fracture of Si due to HF. However, other work<sup>7,16</sup> on crack growth in Si in a variety of settings and environments has not demonstrated reproducible behavior that could be attributed to environmentally enhanced crack growth. Theoretically understanding the ineffectiveness of environmental H<sub>2</sub>O on crack growth in Si will provide valuable information about the effects of environmental molecules in Si-based materials.

A theoretical work by Wong-Ng *et al.*,<sup>17</sup> using the molecular-orbital method, addressed environmental effects of H<sub>2</sub>O on the fracture of Si. In their work, a small hydrogen-terminated Si cluster (Si<sub>8</sub>H<sub>16</sub>) was considered to mimic the atomic structure of Si near the crack tip. Two dangling bonds (DBs) of the Si cluster corresponding to the DBs on the crack surfaces were saturated with H and OH. Their calculation suggests that steric repulsion with the saturating H and OH might inhibit intrusion of additional H<sub>2</sub>O molecules toward the crack tip. To understand chemical reactions of the environmental H<sub>2</sub>O molecules with the crack-tip atoms and to take into account transfer of the reaction energy requires the use of a more realistic atomic-structure model under externally applied stresses.

<sup>a)</sup>Current address: Graduate School of Engineering, Nagoya Institute of Technology, Nagoya 466-8555, Japan.

<sup>b)</sup>Electronic mail: priyav@usc.edu

Environmental H<sub>2</sub>O molecules may affect Si fracture in various ways. For example, a Si–Si bond at the crack front may be oxidized or broken, as follows:



Computer simulation of the environmental H<sub>2</sub>O molecules is useful to study these processes in realistic settings. In performing the simulations, we need to consider surrounding atoms in the neighborhood of the crack tip as well as the reacting atoms. The stress field around the crack tip depends on the macroscopic shape of the system since the field is proportional to  $1/\sqrt{r}$  near the crack tip in linear elastic theory,<sup>1,7</sup> where  $r$  is the distance from the crack tip. The dynamic response of the surrounding atoms may play an important role in absorbing heat produced at the crack tip.

These effects of the surrounding atoms on chemical reactions at the crack tip may be studied efficiently by embedding a quantum-mechanical calculation of the electronic structure within a large-scale classical mechanical atomistic simulation of nuclear motion based on the molecular-dynamics method.<sup>18</sup> We have recently developed a hybrid quantum-mechanical/molecular-dynamics (QMMD) simulation method<sup>19</sup> for parallel computers by combining density functional theory<sup>20</sup> (DFT) for electronic structure and the MD method for nuclear motion. In the hybrid QMMD method, DFT calculations to treat chemically reacting regions are embedded in an MD simulation, in which some of the atoms are described by DFT, whereas others are described by an empirical interatomic potential; that is, by the molecular mechanics<sup>18</sup> (MM). The QM and MM atoms are coupled dynamically with the scaled-position method.<sup>19,21</sup> Various hybrid schemes combining a QM method, such as the molecular-orbital method,<sup>22</sup> and a MM method, have been developed<sup>22</sup> to simulate chemical processes in solution, such as enzymatic reactions. The hybrid QMMD method is an extension of such hybrid QMMM methods applicable to ceramic and semiconductor materials. In the present study, we apply the hybrid QMMD method to a cracked-Si system with environmental H<sub>2</sub>O molecules to investigate chemical reactions of the H<sub>2</sub>O molecules with Si atoms near the crack tip, and their possible effects on fracture initiation.

Section II describes the hybrid QMMD method and the preparation of the initial configurations for our simulations. In Sec. III, results of the simulations are discussed. Concluding remarks are given in Sec. IV.

## II. HYBRID QMMD SIMULATION

Silicon can be produced as a virtually dislocation-free single crystal.<sup>23</sup> Crystalline Si is known to have two principal crack surfaces:<sup>24</sup> the (110) and (111) planes. Experimental values of the critical stress-intensity factor<sup>7</sup>  $K_c$  for the mode-I opening<sup>7</sup> are  $K_c = 0.89 \text{ MPa} \cdot \sqrt{\text{m}}$  for the (110) plane<sup>23</sup> and  $K_c = 0.92 \text{ MPa} \cdot \sqrt{\text{m}}$  for the (111) plane.<sup>24</sup> The critical stress-intensity factor is proportional to the maximal external stress applied to a specimen before it fractures. In the experiments<sup>23</sup> for the (110) plane, the resulting fracture planes are atomically flat, whereas they zigzag in micro-

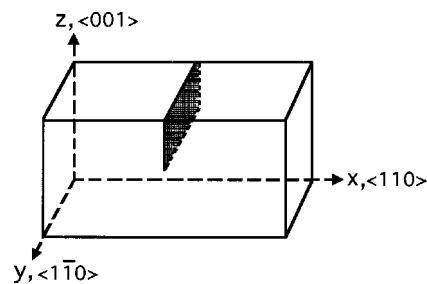


FIG. 1. The Si slab with crystalline directions in the present setting. The hatched half-layer, perpendicular to the  $\langle 110 \rangle$  direction, represents the atomic half-layer that is removed to mimic a straight-edged crack.

scopic scales in the (111) plane.<sup>24</sup> In the present study, we consider the (110) plane for the crack surface.

To prepare a Si model with a crack, we first create a crystalline Si slab of dimensions  $(L_x, L_y, L_z) = (153, 46, 68 \text{ \AA})$ , respectively; the  $x$ ,  $y$ , and  $z$  axes are parallel to the  $\langle 110 \rangle$ ,  $\langle 1\bar{1}0 \rangle$ , and  $\langle 001 \rangle$  directions, respectively. We remove half of the atomic layer parallel to (110) from the center  $[(x, z) = (L_x/2, L_z/2)]$  of the slab to mimic a straight-edged crack, with the crack-front line in the  $\langle 1\bar{1}0 \rangle$  direction (see Fig. 1). Our system is periodic in the  $x$  and  $y$  directions, whereas the free boundary conditions are applied in the  $z$  direction. Before starting the simulation, the system is uniformly stretched by 3% and 4% along the  $x$  direction to obtain the stress intensity factors of  $0.4 \text{ MPa} \cdot \sqrt{\text{m}}$  and  $0.5 \text{ MPa} \cdot \sqrt{\text{m}}$ , respectively. The system is relaxed to zero temperature by scaling the atomic velocities in the MD simulation using the Stillinger–Weber interatomic potential.<sup>25</sup> Up to this stage, we have no quantum atoms, and the Hamiltonian of the system is

$$H_{\text{MD}} = \sum_i m |\dot{\mathbf{r}}_i|^2/2 + \sum_{i<j} V_2(\mathbf{r}_i, \mathbf{r}_j) + \sum_{i<j<k} V_3(\mathbf{r}_i, \mathbf{r}_j, \mathbf{r}_k), \quad (1)$$

where  $m$  is the mass of a silicon atom.

After the initial setup of creating a crack in silicon, we select clusters of atoms (i.e., QM atoms) from the classical MD atoms near the crack tip and treat the valence electrons of the selected atoms quantum mechanically. We now briefly summarize our hybrid QMMD simulation scheme, the details of which are explained in our previous papers.<sup>19,21,26</sup> The total Hamiltonian of such a hybrid QMMD system is written in a modular form as

$$H = H_{\text{MD}} + \sum_{\text{cluster}} [E_{\text{QM}}^{\text{cluster}}(\{\mathbf{r}_{\text{QM}}\}, \{\mathbf{r}_{\text{HS}}\}) - E_{\text{MD}}^{\text{cluster}}(\{\mathbf{r}_{\text{QM}}\}, \{\mathbf{r}_{\text{HS}}\})], \quad (2)$$

where the last two terms on the right-hand side of Eq. (2) represent the QM correction to the MM potential energy for each cluster of QM atoms. The  $\{\mathbf{r}_{\text{QM}}\}$  in Eq. (2) are the nuclear positions of the QM atoms; the  $\{\mathbf{r}_{\text{HS}}\}$  are the positions of “handshake” (HS) atoms, which are classical atoms bonded to a QM atom. In the quantum calculation, each bond connecting a QM atom and a HS atom is terminated by H. The positions of the termination-H atoms are determined dy-

namically with the scaled-position method<sup>19,21</sup> as a function of  $\{\mathbf{r}_{\text{QM}}\}$  and  $\{\mathbf{r}_{\text{HS}}\}$ . The total Hamiltonian  $H$  is conserved during the hybrid simulation. Thermal energies produced as a result of chemical reaction in the QM regions are transferred to the surrounding MM region.

Electronic structure of a QM cluster with termination-H atoms is described by DFT. In the Kohn–Sham (KS) formulation, the total energy of the cluster of atoms with their nuclear coordinates  $\{\mathbf{r}\}$  is written as<sup>20</sup>

$$E_{\text{QM}}^{\text{cluster}}(\{\mathbf{r}\}) = - \sum_{i=1}^{\text{occupied}} \psi_i^* \Delta \psi_i d\mathbf{x} + \frac{1}{2} \int \int \frac{\rho(\mathbf{x})\rho(\mathbf{x}')}{|\mathbf{x}-\mathbf{x}'|} d\mathbf{x}d\mathbf{x}' + \int V_{\text{ion}}(\mathbf{x})\rho(\mathbf{x})d\mathbf{x} + E_{\text{xc}}(\rho) + E_{\text{ion}}(\{\mathbf{r}\}), \quad (3)$$

where  $\{\psi_i\}$  are the KS orbitals, and  $\rho(x) = 2 \sum_{i=1}^{\text{occupied}} |\psi_i(\mathbf{x})|^2$  is the charge density of the valence electrons. The  $V_{\text{ion}}$  in Eq. (3) is the pseudopotential for valence electrons;  $E_{\text{xc}}$  and  $E_{\text{ion}}$  are the exchange–correlation energy and the interaction energy between ion cores, respectively. The generalized gradient approximation by Perdew, Burke, and Ernzerhof<sup>27</sup> is adopted for  $E_{\text{xc}}$ . The KS wave functions are orthonormal:  $\int \psi_i^* \psi_j d\mathbf{x} = \delta_{ij}$ . Atomic units are used and only doubly occupied orbitals are considered in Eq. (3). Cartesian mesh-points in real coordinates are used to calculate derivatives of the wave functions in Eq. (3) by the finite-difference method.<sup>19,21,28</sup> For efficient implementation on parallel computers, data on the mesh-points are spatially decomposed and stored in parallel compute-nodes.<sup>19,21</sup> Equation (3) may be regarded as a nonlinear constrained-minimization problem. Variation of Eq. (3) with respect to  $\psi_i$  gives the KS equation

$$\left[ -\frac{\Delta}{2} + V_{\text{Hartree}}(\mathbf{x}) + V_{\text{ion}}(\mathbf{x}) + \frac{\delta E_{\text{xc}}}{\delta \rho(\mathbf{x})} \right] \psi_i = e_i \psi_i, \quad (4)$$

with the Hartree equation  $\Delta V_{\text{Hartree}}(\mathbf{x}) = -4\pi\rho(\mathbf{x})$ . Numerical solutions of the equations on the mesh-points are accelerated with the multigrid method<sup>19,21,29</sup> and the double-grid method.<sup>30</sup>

In the present hybrid QMMD simulation, we select three QM regions from the total system and calculate their electronic structures by the DFT. Each QM region comprises 36 Si atoms around the crack front before putting a water molecule in each QM region. The centers of the QM region are aligned along the crack-front line, as depicted in Fig. 2. The DFT calculation is performed for each atomic cluster (i.e., QM cluster) consisting of the 36 Si atoms selected and 40 termination-H atoms introduced to minimize termination effects. [The total number of atoms in the three DFT calculations is thus  $(36+40) \times 3 = 228$ , before water molecules are inserted.] There exist four dangling bonds in each QM cluster, corresponding to the unsaturated crack surfaces.

The switch from the purely classical Hamiltonian ( $H_{\text{MD}}$ ) to the hybrid one ( $H$ ) necessitates further relaxation to stabi-

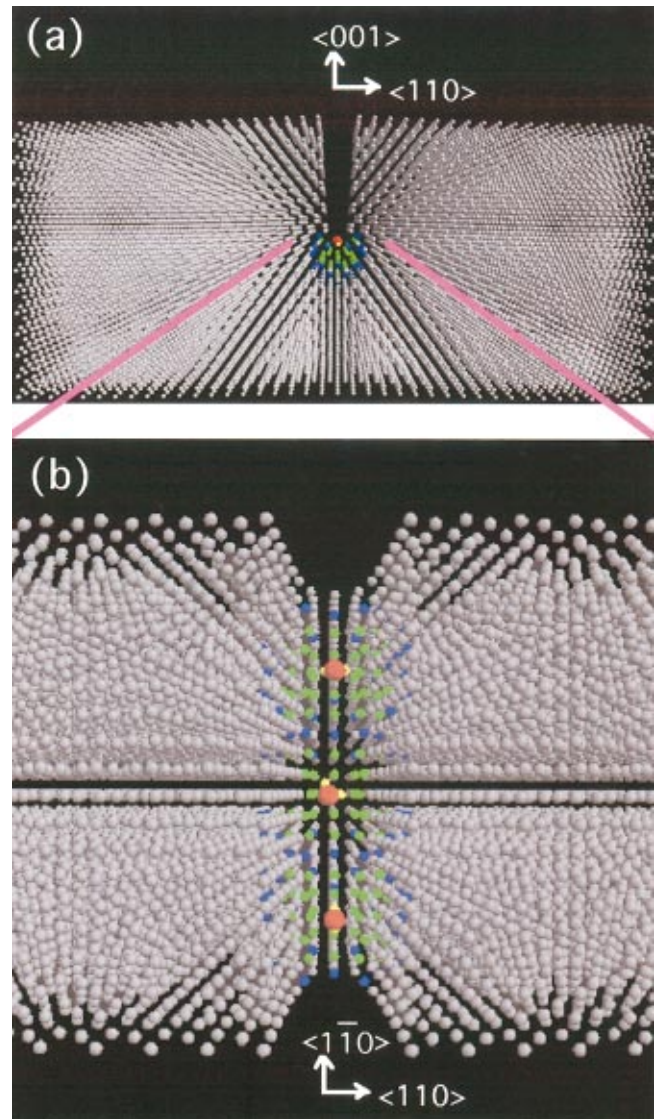


FIG. 2. (Color) (a) The total system for the  $K=0.4 \text{ MPa} \cdot \sqrt{\text{m}}$  case viewed from the  $\langle 1\bar{1}0 \rangle$  direction. (b) Close-up of the crack-front region in the same system viewed from the  $\langle 001 \rangle$  direction. Green spheres represent QM Si atoms; blue, HS Si atoms; red, QM O atoms; yellow, QM H-atoms; gray, MM Si atoms.

lize the hybrid system. Hybrid QMMD simulation runs are performed for 3% and 4% uniaxial strains, with a velocity scaling-factor of 0.95 at every time step of 2.0 fs until the temperature of every atom becomes less than 0.01 K. The smallest grid size used in DFT calculation is 0.21 a.u. in real space. The resulting atomic configuration and its close-up around the crack-front region for 3% strain are shown in Figs. 2 and 3, respectively. In Figs. 2 and 3, QM Si atoms are drawn as green spheres, HS Si atoms as blue spheres, and classical Si atoms as gray spheres.

To compare our simulations results with experiments, it is useful to evaluate the stress-intensity factor<sup>7</sup>  $K$  for the 3%- and 4%-stretched cases. Using the formula<sup>31</sup>  $K = \alpha \sqrt{\pi c} |\sigma_{xx}|$  for uniform applied stresses (mode I) with the edge correction factor  $\alpha \sim 1.12$ , the crack depth  $c = 34 \text{ \AA}$ , and the stress  $|\sigma_{xx}| = 3.2 \text{ GPa}$ , we may evaluate  $K \sim 0.4 \text{ MPa} \cdot \sqrt{\text{m}}$  for the 3%-stretched case and  $K \sim 0.5 \text{ MPa} \cdot \sqrt{\text{m}}$  for the

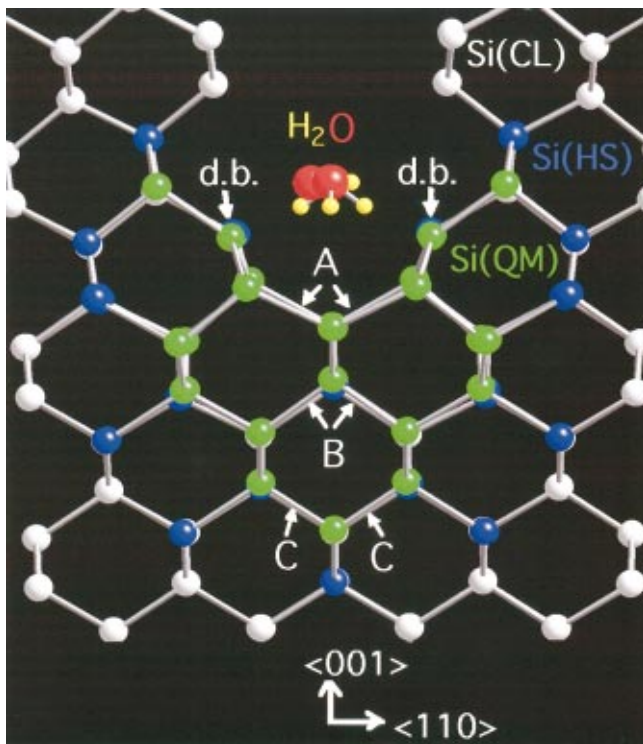


FIG. 3. (Color) Close-up of the crack-front region viewed from the  $\langle 1\bar{1}0 \rangle$  direction. Green spheres represent QM Si atoms; blue, HS Si atoms; red, QM O atoms; yellow, QM H atoms; gray, MM Si atoms. Silicon atoms with dangling bonds are marked by d.b.

4%-stretched case. To characterize strain relaxation at the crack front, we define three types (A, B, and C) of Si-Si pairs (see Fig. 3). The numbers of type A, B, and C Si-Si pairs in each QM cluster are 6, 4, and 2, respectively. Length  $d$  of the Si-Si pair is stretched most for the type A pairs at the crack front. The  $d$  of the type A pair are 2.42 Å for  $K = 0.4 \text{ MPa} \cdot \sqrt{\text{m}}$  and 2.59 Å for  $K = 0.5 \text{ MPa} \cdot \sqrt{\text{m}}$ ; it is 5% and 13% longer, respectively, than the crystalline value 2.30 Å.

To investigate possible effects of H<sub>2</sub>O molecules on fracture initiation, we put a H<sub>2</sub>O molecule in each QM region. The H<sub>2</sub>O molecules are added with zero velocity and random orientation, at a position separated by 4.0 Å in the  $\langle 001 \rangle$  direction from the central Si atom at the crack front. The total number of atoms used in the DFT calculations is 237; that is, each of the three QM clusters contains 79 atoms, composed of 36 Si, 40 termination-H, one O, and two H atoms. Initial configuration of our hybrid simulation for the environmental effects of H<sub>2</sub>O molecules is shown in Figs. 2 and 3 for the  $K = 0.4 \text{ MPa} \cdot \sqrt{\text{m}}$  case. The H<sub>2</sub>O molecules are drawn with red (O) and yellow (H) spheres in Figs. 2 and 3. The time step is 1.0 fs in the simulation, which is half of the value used in the relaxation run before inserting water molecules and is sufficiently small to follow the atomic motion. Hybrid QMMD simulation runs for  $K = 0.4 \text{ MPa} \cdot \sqrt{\text{m}}$  and  $0.5 \text{ MPa} \cdot \sqrt{\text{m}}$  are performed on 49 compute-nodes of a parallel computer. A single compute-node is assigned to the MD computation, while 16 compute-nodes each are assigned to the computation of the three QM clusters. The simulation runs are performed for ~500 fs.

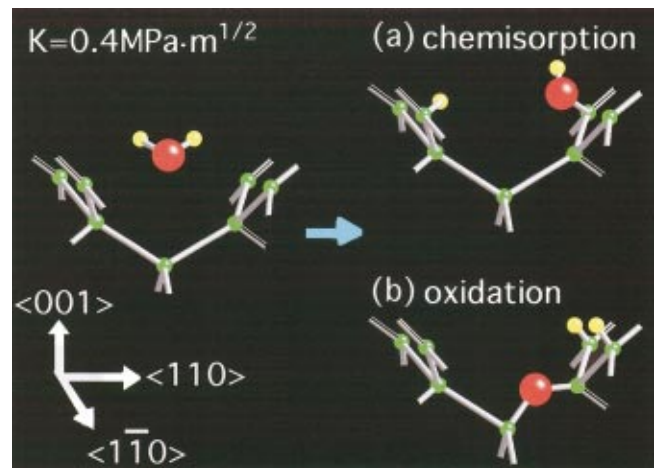


FIG. 4. (Color) Schematic drawing of two types of reaction processes found in the present simulation run with  $K = 0.4 \text{ MPa} \cdot \sqrt{\text{m}}$ .

### III. RESULTS AND DISCUSSION

Our simulations reveal three different types of chemical reactions between three H<sub>2</sub>O molecules and Si atoms at the crack tip, which are depicted in Figs. 4 and 5. In the  $K = 0.4 \text{ MPa} \cdot \sqrt{\text{m}}$  case, two of the three H<sub>2</sub>O molecules dissociate into H and OH and adhere to DB sites on the crack surface [Fig. 4(a), chemisorption]. The other H<sub>2</sub>O molecule dissociates into 2H and O, and then the two H atoms adhere to two DB sites on the crack surface, while O is inserted between a Si-Si pair at the crack front [Fig. 4(b), oxidation]. In the  $K = 0.5 \text{ MPa} \cdot \sqrt{\text{m}}$  case, two H<sub>2</sub>O molecules dissociate into 2H and O and oxidation process follows [Fig. 5(a), oxidation]. The third H<sub>2</sub>O molecule dissociates into H and OH, and the H adheres to a DB site, while OH breaks the Si-Si bond at the crack front [Fig. 5(b), bond breakage].

Figure 6 shows the time evolution of Si-Si separation  $d$  for the type A, B, and C silicon pairs in the  $K = 0.4 \text{ MPa} \cdot \sqrt{\text{m}}$  case. The type A, B, and C pairs are located along the crack extension direction, as shown in Fig. 3. Separation between the type A and C pairs along the  $\langle 001 \rangle$  direction is 5.3 Å. It is expected that sequential propagation of

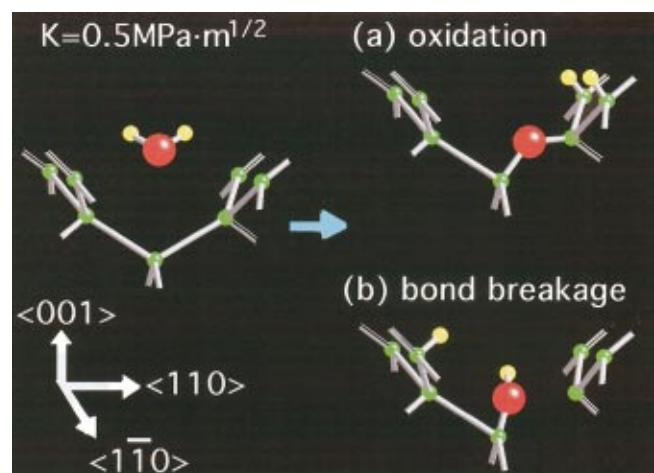


FIG. 5. (Color) Schematic drawing of two types of reaction processes found in the present simulation run with  $K = 0.5 \text{ MPa} \cdot \sqrt{\text{m}}$ .

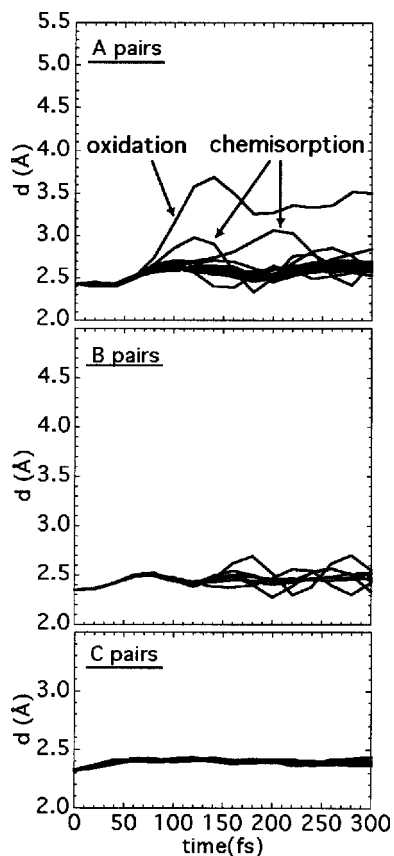


FIG. 6. Time evolution of Si-Si bond distance  $d$ , for type A, B, and C silicon pairs in the  $K=0.4 \text{ MPa}\cdot\sqrt{\text{m}}$  case. The type A, B, and C pairs are located along the crack-extension direction, as shown in Fig. 3. The numbers of type A, B, and C Si-Si pairs are 18, 12, and 6, respectively.

$d$ -extension toward the type C pairs will be seen if fracture is initiated due to the  $\text{H}_2\text{O}$  molecule. Initial values of  $d$  for the type A, B, and C pairs are 2.42, 2.35, and 2.31 Å, respectively, in the  $K=0.4 \text{ MPa}\cdot\sqrt{\text{m}}$  case. Due to thermal fluctuations, values of  $d$  for the type B and C pairs oscillate around their equilibrium values, with fluctuation widths 0.1–0.4 Å for the type B and 0.1 Å for the type C pairs. Values of  $d$  for the type A pairs also oscillate, except for one pair whose  $d$  extends to  $\sim 3.3$  Å, reflecting insertion of O between the Si-Si pair, leading to the formation of a Si-O-Si structure.

Figure 7 shows the corresponding results for the  $K=0.5 \text{ MPa}\cdot\sqrt{\text{m}}$  case. Initial values of  $d$  for the type A, B, and C silicon pairs are 2.59, 2.48, and 2.40 Å, respectively. Two type A pairs form Si-O-Si structures because of the oxidation process, and the third type A pair is broken at  $\sim 250$  fs, as seen in Fig. 7 (top). The bond breakage of the type A pair is accompanied by that of a type B pair in Fig. 7 (middle). The Griffith value<sup>7</sup>  $K^G$  for the stress-intensity factor calculated using the surface energy is  $K^G=0.45 \text{ MPa}\cdot\sqrt{\text{m}}$  for the present setting.<sup>32</sup> Since  $K^G \leq K$  in this simulation, crack propagation due to such bond breakage may be expected. However, such bond breakage does not propagate to the type C pairs, as seen in Fig. 7 (bottom). We find in the  $K=0.5 \text{ MPa}\cdot\sqrt{\text{m}}$  case that only one  $\text{H}_2\text{O}$  acts to break a Si-Si bond; the other two  $\text{H}_2\text{O}$  molecules form the Si-O-Si structures. The formation of the Si-O-Si structures may reduce

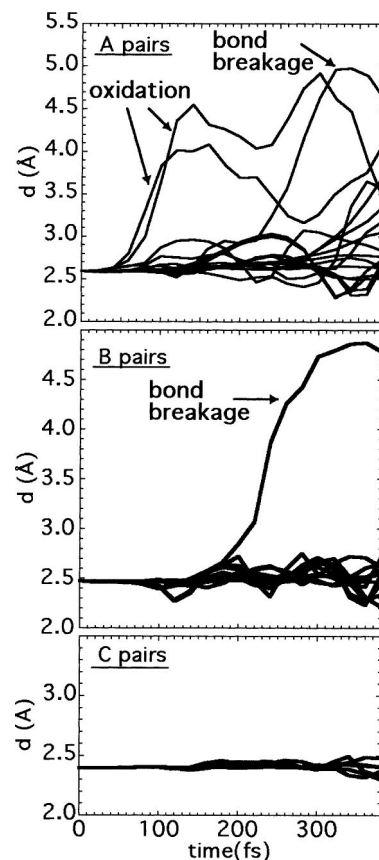


FIG. 7. Time evolution of Si-Si bond distance  $d$  for type A, B, and C silicon pairs in the  $K=0.5 \text{ MPa}\cdot\sqrt{\text{m}}$  case. The type A, B, and C pairs are located along the crack-extension direction, as shown in Fig. 3. The numbers of type A, B, and C Si-Si pairs are 18, 12, and 6, respectively.

the tensile stress at the crack tip and hence act to hinder crack extension.

Degrees of charge transfer between reacting atoms are useful quantities to understand the reaction mechanisms. We evaluate the gross charge of each atom through the Mulliken population analysis<sup>33,34</sup> by projecting the KS wave functions to the atomic ones in vacuum. Figure 8 depicts time evolution of the charges of the QM atoms for the chemisorption process in the  $K=0.4 \text{ MPa}\cdot\sqrt{\text{m}}$  case as viewed from the  $\langle 001 \rangle$  direction. The color on atoms represents the atomic charge. As the OH created by the decomposition of  $\text{H}_2\text{O}$  adheres to a DB site of Si for 100–300 fs, the charge of O becomes more negative by  $0.2e$ . The corresponding data for the oxidation process in the  $K=0.4 \text{ MPa}\cdot\sqrt{\text{m}}$  case are shown in Fig. 9. As an O atom is inserted between a Si-Si pair, the charges of the Si atoms become more positive by  $0.3e$ . Figure 10 depicts the bond-breakage process in the  $K=0.5 \text{ MPa}\cdot\sqrt{\text{m}}$  case. In the process, the charge of O becomes more negative by  $0.3e$  as OH breaks a Si-Si bond. Both in the chemisorption (Fig. 8) and the bond-breakage (Fig. 10) processes, one of the H atoms becomes more positive by  $0.2e$ . Decomposition of a  $\text{H}_2\text{O}$  molecule into H and OH in those processes (see Figs. 4 and 5) enhances transferring of electron between neighboring H and O in OH.

In all the three processes in Figs. 8–10, we find that the O atom attracts electrons from the neighboring Si atoms. In

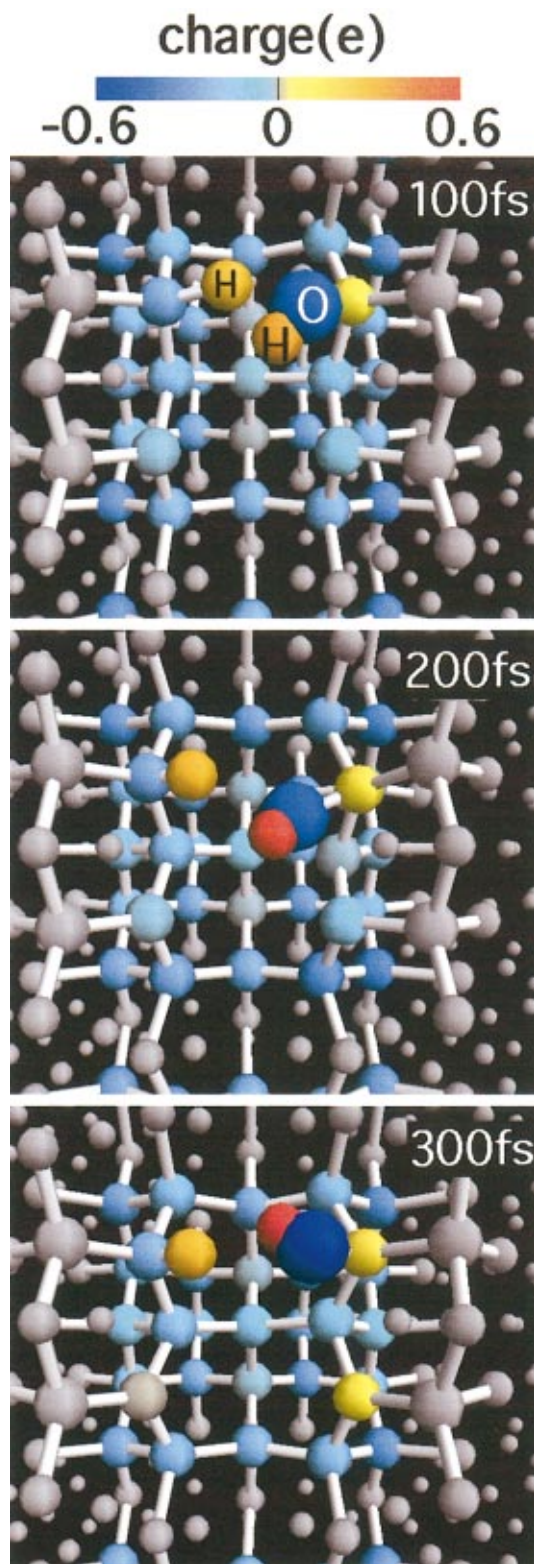


FIG. 8. Time evolution of the charges of the QM atoms for the chemisorption process (see Fig. 6) in the  $K=0.4 \text{ MPa} \cdot \sqrt{\text{m}}$  case viewed from the  $\langle 001 \rangle$  direction. The color of the atoms represents the atomic charge. Three atoms forming the  $\text{H}_2\text{O}$  molecule at the initial, are indicated in the top panel. The O charge becomes more negative by  $0.2e$  during 100–300 fs.

Figs. 9 and 10, the O atom moves toward the bonding electrons residing initially between neighboring two Si atoms and forming the covalent bond. Subsequent transferring of the electrons to the O atom may break the Si–Si bond if it is

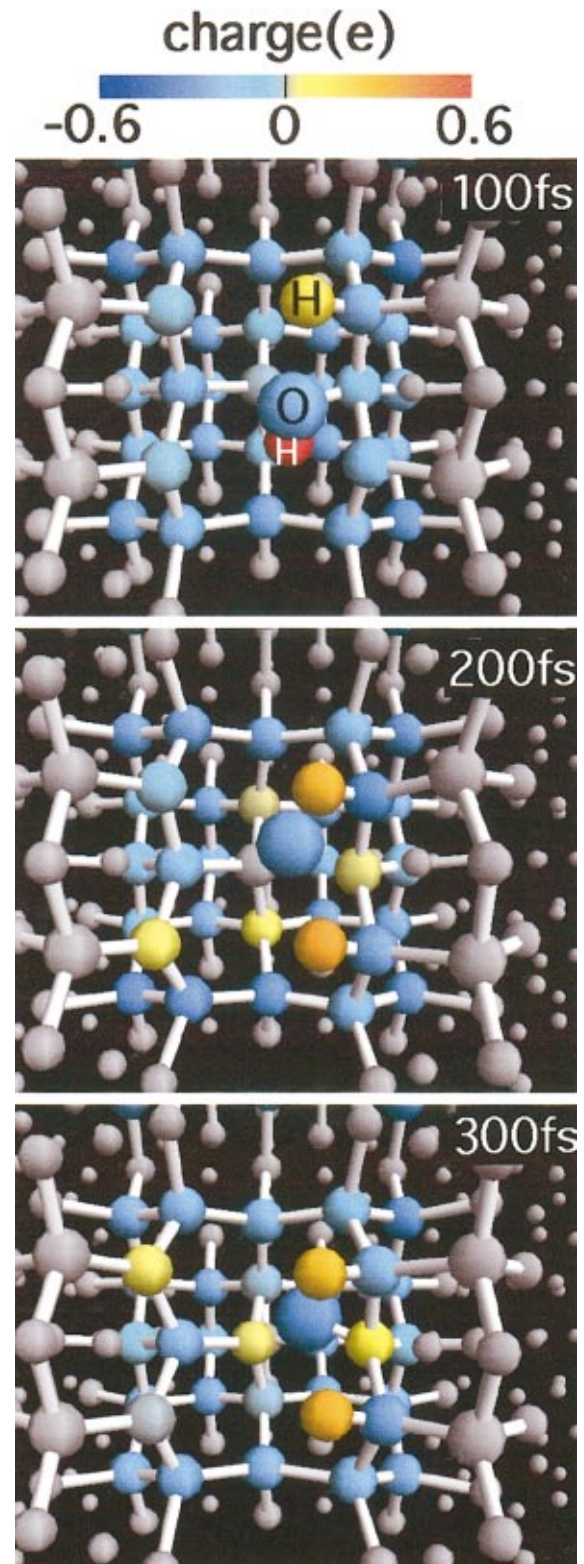


FIG. 9. Time evolution of the charges of the QM atoms for the oxidation process (see Fig. 6) in the  $K=0.4 \text{ MPa} \cdot \sqrt{\text{m}}$  case viewed from the  $\langle 001 \rangle$  direction. The color of the atoms represents the atomic charge. Three atoms forming the  $\text{H}_2\text{O}$  molecule at the initial, are indicated in the top panel. The two Si atoms connecting to O as Si–O–Si become more positive by  $0.3e$  during 100–300 fs.

strongly stretched with  $K=0.5 \text{ MPa} \cdot \sqrt{\text{m}}$ , as depicted in Fig. 10. While only formation of Si–O–Si may occur if the Si–Si bond is weakly stretched with  $K=0.4 \text{ MPa} \cdot \sqrt{\text{m}}$ , as shown in Fig. 9.

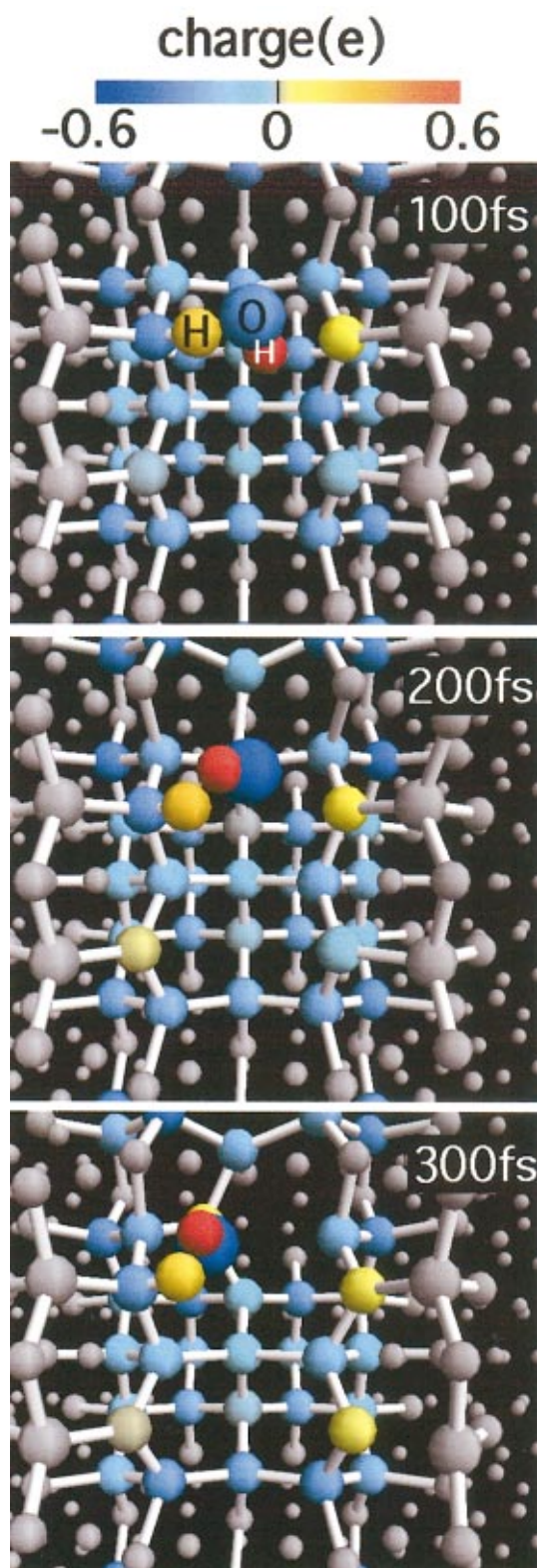


FIG. 10. Time evolution of the charges of the QM atoms for the bond-breakage process (see Fig. 7) in the  $K=0.5 \text{ MPa} \cdot \sqrt{\text{m}}$  case viewed from the  $\langle 001 \rangle$  direction. The color of the atoms represents the atomic charge. Three atoms forming the  $\text{H}_2\text{O}$  molecule at the initial, are indicated in the top panel. The O charge becomes more negative by  $0.3e$  as OH breaks a Si–Si bond during 100–300 fs.

#### IV. CONCLUDING REMARKS

In summary we have performed hybrid QMMD simulations of silicon with a crack under tension ( $K$

$=0.4 \text{ MPa} \cdot \sqrt{\text{m}}$  and  $0.5 \text{ MPa} \cdot \sqrt{\text{m}}$ ) with three  $\text{H}_2\text{O}$  molecules, to investigate possible environmental effects on fracture initiation. The DFT calculations were applied to three clusters of atoms that include three  $\text{H}_2\text{O}$  molecules, 108 Si atoms around the crack front, and 120 termination-H atoms (in total, 237 atoms). Those QM atoms were coupled dynamically to the surrounding MD Si atoms. The simulation results exhibited significant effects of  $K$  on the reaction of  $\text{H}_2\text{O}$  molecules at a crack tip. In the  $K=0.4 \text{ MPa} \cdot \sqrt{\text{m}}$  case, the  $\text{H}_2\text{O}$  molecule either dissociated into H and OH to adhere to the crack surface or oxidized Si to form a Si–O–Si structure ( $\text{Si–Si} + \text{H}_2\text{O} \rightarrow \text{Si–O–Si} + 2\text{H}$ ). In the  $K=0.5 \text{ MPa} \cdot \sqrt{\text{m}}$  case, on the other hand, we found the  $\text{H}_2\text{O}$  molecules either oxidized Si or broke a Si–Si bond ( $\text{Si–Si} + \text{H}_2\text{O} \rightarrow \text{Si–OH} + \text{Si} + \text{H}$ ). Analyses of the degrees of charge transfer between the QM atoms were carried out to understand the reaction mechanisms.

In the present study, we have considered only (110) crack surface of pure Si (i.e., with no surface saturation atoms) to study the environmental effects of  $\text{H}_2\text{O}$  molecules. In experiments, depending on preparation procedures, crack surfaces can be partially saturated by H or other elements.<sup>35,36</sup> Hybrid QMMD simulations are in progress to study the environmental effects for different crack planes with varying surface conditions. We are also planning to perform hybrid simulations of the environmental effects of various molecules for alumina, for which significant environmental effects on fracture have been reported.<sup>7,37</sup> Comparison of these simulation results will give us a broad and detailed understanding of the environmental effects on fracture in semiconducting and ceramic materials.

#### ACKNOWLEDGMENTS

Simulations were performed on an SGI 2800 at the Institute for Solid State Physics at the University of Tokyo, parallel supercomputers at DoD Major Shared Resource Centers under CHSII and Challenge projects, and PC clusters at the Concurrent Computing Laboratory for Materials Simulations at Louisiana State University and Yamaguchi University. The work at Yamaguchi is supported by ACT-JST. The work at USC is partially supported by NSF, DOE, ARL, AFRL, NASA, and AFOSR-DURINT:USC-Berkeley-Princeton.

<sup>1</sup>D. R. H. Jones, *Engineering Materials 3, Materials Failure Analysis* (Pergamon, New York, 1993).

<sup>2</sup>*Proceedings of the 12th International Conference on Microelectromechanical Systems* (IEEE, New York, 1999).

<sup>3</sup>*Nanotechnology Research Directions, IWGN Workshop Report*, edited by M. C. Roco, S. Williams, and P. Alvisatos (Int'l Technology Research Inst., Loyola College, Baltimore, 1999); <http://itri.loyola.edu/nano/IWGN.Research.Directions/>

<sup>4</sup>A. Nakano *et al.*, *IEEE Trans. Electron Devices* **47**, 1804 (2000).

<sup>5</sup>Q. T. Zhao, F. Klinkhammer, M. Dolle, L. Kappius, and S. Mantl, *Appl. Phys. Lett.* **74**, 454 (1999).

<sup>6</sup>C. Muhlstein, S. Brown, and R. O. Ritchie, *Sens. Actuators, A* **94**, 177 (2001).

<sup>7</sup>B. Lawn, *Fracture of Brittle Solids*, 2nd Ed. (Cambridge University Press, New York, 1995).

<sup>8</sup>S. M. Wiederhorn and P. R. Townsend, *J. Am. Ceram. Soc.* **55**, 99 (1970).

<sup>9</sup>G. L. Cheeseman and B. R. Lawn, *Phys. Status Solidi* **3**, 951 (1970).

<sup>10</sup>T. A. Michalske and E. R. Fuller, *J. Am. Ceram. Soc.* **11**, 586 (1985).

- <sup>11</sup>T. A. Michalske and S. W. Freiman, *Nature (London)* **259**, 511 (1981).
- <sup>12</sup>D. G. Truhlar and V. McKoy, *Comput. Sci. Eng.* **2**(6), 19 (2000).
- <sup>13</sup>C. Winstead and V. McKoy, *Comput. Phys. Commun.* **128**, 386 (2000).
- <sup>14</sup>Y.-M., Chiang, D. Birnie III, and W. D. Kingery, *Physical Ceramics* (Wiley, New York, 1997).
- <sup>15</sup>M. D. Thouless and R. F. Cook, *Appl. Phys. Lett.* **56**, 1962 (1990).
- <sup>16</sup>T. J. Chuang, *J. Am. Ceram. Soc.* **70**, 162 (1989).
- <sup>17</sup>W. Wong-Ng, G. S. White, S. W. Freiman, and C. G. Lindsay, *Comput. Mater. Sci.* **6**, 63 (1996).
- <sup>18</sup>D. Frenkel and B. Smit, *Understanding Molecular Simulation* (Academic, New York, 1996).
- <sup>19</sup>S. Ogata, F. Shimojo, A. Nakano, P. Vashishta, and R. K. Kalia, *Comput. Phys. Commun.* **149**, 30 (2002).
- <sup>20</sup>P. Hohenberg and W. Kohn, *Phys. Rev.* **136**, B864 (1964); W. Kohn and L. J. Sham, *ibid.* **140**, A1133 (1965); W. Kohn and P. Vashishta, in *Inhomogeneous Electron Gas*, edited by N. H. March and S. Lundqvist (Plenum, New York, 1983), p. 79.
- <sup>21</sup>S. Ogata, E. Lidorikis, F. Shimojo, A. Nakano, P. Vashishta, and R. K. Kalia, *Comput. Phys. Commun.* **138**, 143 (2001).
- <sup>22</sup>See, e.g., J. Gao and D. G. Truhlar, *Annu. Rev. Phys. Chem.* **53**, 467 (2002).
- <sup>23</sup>G. Michot, *Cryst. Prop. Prep.* **17–18**, 55 (1989).
- <sup>24</sup>A. George and G. Michot, *Mater. Sci. Eng., A* **164**, 118 (1993).
- <sup>25</sup>F. H. Stillinger and T. A. Weber, *Phys. Rev. B* **31**, 5262 (1985).
- <sup>26</sup>A. Nakano, M. E. Bachlechner, R. K. Kalia, E. Lidorikis, P. Vashishta, G. Z. Voyiadjis, T. J. Campbell, S. Ogata, and F. Shimojo, *Comput. Sci. Eng.* **3**, 56 (2001); H. Kikuchi, R. K. Kalia, A. Nakano, P. Vashishta, H. Iyotomi, S. Ogata, T. Kouno, F. Shimojo, K. Tsuruta, and S. Saini, in *Proc. Supercomputing 2002* (IEEE Computer Society, Los Alamitos, CA, 2002).
- <sup>27</sup>J. P. Perdew, K. Burke, and M. Ernzerhof, *Phys. Rev. Lett.* **77**, 3865 (1996).
- <sup>28</sup>J. R. Chelikowsky, N. Troullier, and Y. Saad, *Phys. Rev. Lett.* **72**, 1240 (1994).
- <sup>29</sup>A. Brandt, *Math. Comput.* **31**, 333 (1977); J.-L. Fattebert and J. Bernholc, *Phys. Rev. B* **62**, 1713 (2000); T. L. Beck, *Rev. Mod. Phys.* **72**, 1041 (2000).
- <sup>30</sup>T. Ono and K. Hirose, *Phys. Rev. Lett.* **82**, 5016 (1999).
- <sup>31</sup>See, e.g., Eq. (2.20) in Ref. 7.
- <sup>32</sup>R. Pérez and P. Gumbsch, *Acta Mater.* **48**, 4517 (2000).
- <sup>33</sup>R. S. Mulliken, *J. Chem. Phys.* **23**, 1833 (1955).
- <sup>34</sup>D. Sánchez-Portal, E. Artacho, and J. M. Soler, *J. Phys.: Condens. Matter* **8**, 3859 (1996).
- <sup>35</sup>P. A. Thiel and T. E. Madey, *Surf. Sci. Rep.* **7**, 211 (1987).
- <sup>36</sup>H. N. Waltenberg and J. T. Yates, Jr., *Chem. Rev. (Washington, D.C.)* **95**, 1589 (1995).
- <sup>37</sup>B. R. Lawn, *J. Mater. Sci.* **15**, 1207 (1980).